A Well-Balanced and Non-Negative Numerical Scheme for Solving the Integrated Shallow Water and Solute Transport Equations

Qiuhua Liang*

School of Civil Engineering and Geosciences, Newcastle University, Newcastle upon Tyne, NE1 7RU, England, UK.

Abstract. Based on the recent development in shallow flow modelling, this paper presents a finite volume Godunov-type model for solving a 4×4 hyperbolic matrix system of conservation laws that comprise the shallow water and depth-averaged solute transport equations. The adopted governing equations are derived to preserve exactly the solution of lake at rest so that no special numerical technique is necessary in order to construct a well-balanced scheme. The HLLC approximate Riemann solver is used to evaluate the interface fluxes. Second-order accuracy is achieved using the MUSCL slope limited linear reconstruction together with a Runge-Kutta time integration method. The model is validated against several benchmark tests and the results are in excellent agreement with analytical solutions or other published numerical predictions.

AMS subject classifications: 76R99, 65E99

Key words: Solute transport, shallow water equations, advection-diffusion equation, well-balanced scheme, wetting and drying, source terms, Riemann solver.

1 Introduction

Solute transport is a common process that may take place in rivers, lakes and estuarine and coastal areas where the flows have horizontal dimensions much larger than their vertical extent (shallow flows). It may be closely related to the water quality in these shallow water bodies and have great impacts on the local environment and ecosystem. It may also cause potential risk on public health and local economy, e.g. when it is associated with an urban flood event. To understand the solute transport process in a shallow flow is thus of fundamental and practical importance to hydraulic and environmental

---

*Corresponding author. *Email address:* `Qiuhua.Liang@ncl.ac.uk` (Q. Liang)

engineering. In this work, we consider the passive solute transport driven by shallow flows, where 'passive' essentially means that the solute particles (or concentration) are drifted by the fluid velocity and their feedback to the flow is negligible. This assumption is realistic for most of the engineering problems with low solute concentration.

In practice, it is common to assume that shallow flows are predominantly horizontal with hydrostatic pressure distribution so that they can be mathematically described by the 2D shallow water equations. For solute transport, if the pollutant is vertically well-mixed, their dynamics may be represented by a depth-averaged advection-diffusion equation [17, 39]. Taking place in domains with irregular geometries and topographies, shallow flows are normally hydrodynamically complex and the associated solute particles are hence subject to random and complicated movement. Therefore, analytical solutions to these governing equations are generally impossible to obtain and numerical methods must be employed. Accurate numerical modelling thus provides an essential tool for water quality management, environmental impact assessment and hydraulic design [14].

It is not easy to design an accurate and efficient numerical model for solving the shallow water and advection-diffusion equations as both the flow and solute concentration may be non-smooth and contain simultaneously nonlinear bore and rarefaction waves and linear discontinuities [12]. Traditionally, a decoupled strategy is often used, i.e. the flow field is first obtained by analytical, numerical or experimental approaches and then used to drive the solute motions [3, 10, 12, 17, 31, 33]. However, Murillo et al. [34] implies that a coupling system provides a better choice in avoiding numerical instabilities in the solute concentration when it is applied to simulate complex situations where solute transport occurs in natural environmental flows with steep or even discontinuous gradients.

When discussing the Godunov-type numerical scheme for solving the 2D shallow water equations, Toro [39] suggested that the behaviour of the advection-diffusion equation for passive transport problems is identical to that of the *y*-direction momentum equation in the Riemann solution structure. This idea was adopted by Liang et al. [28] and they integrated the advection-diffusion equation into a pre-balanced formulation of the 2D shallow water equations to form a 4×4 hyperbolic matrix system of conservation laws. The numerical properties of the coupled system are identical to the hyperbolic shallow water equations and so most of the modern numerical techniques developed for the shallow water equations can be directly applied to solve the new 4×4 system. Liang et al. [23] solved the coupled hyperbolic conservation laws using a finite volume Godunov-type scheme on adaptive quadtree grids. This coupling strategy was also used by Murillo et al. [34] in which the integrated shallow water and solute transport equations were solved by a first-order Godunov-type scheme on unstructured grids. The scheme was later extended to include applications involving wetting and drying over complex domains [35]. A similar coupled system is also solved by Benkhaldoun et al. [4] using a non-homogeneous Riemann solver for applications involving complex bed topographies.

As mentioned before, the numerical techniques derived for the shallow water equa-

tions may be directly applied to solve the integrated system of shallow water and solute transport equations. Zhao et al. [42] pointed out that a good 2D shallow flow model should be able to handle complex topography, repeatedly wetting and drying, high roughness value, steady or unsteady flow and flow involving different regimes (e.g. transcritical flow). All of these aspects have received intensive attentions in the past three decades and numerous mathematical and numerical techniques have been reported in literature. Godunov-type methods have gradually become a standard in solving the shallow water equations as they provide solutions that admit different regimes for both steady and unsteady flows [13, 32, 39]. In dealing with complex domain topography, a numerical scheme should be well-balanced, i.e. preserving the solution of lake at rest. Since the pioneer work of Bermúdez and Vázquez [5] and Greenberg and LeRoux [19], a number of well-balanced numerical schemes for shallow water equations have been presented [1,18,23,25,27,29,37,41,43,44] and the list is far from complete. Notable efforts were made by Rogers et al. [37], Liang and Borthwick [27] and Liang and Marche [29] where new formulation of shallow water equations were derived to accept well-balanced solutions so that no special numerical technique is needed. The pre-balanced shallow water equations presented by Liang and Borthwick [27] and Liang and Marche [29] also facilitate applications to wetting and drying.

For wetting and drying, a common approach is to add small water depth in the dry cells to avoid direct calculation of wet-dry interface. However, as Toro [39] pointed out, this approach is physically incorrect and may ruin the numerical solution near the wet-dry front. Numerical schemes directly computing wet-dry front have been developed [3, 6, 7, 27]. However, most of these models predict negative water depth near the wet-dry front and thus affect the numerical stability. In order to maintain stability, a normal way is to modify the flow variables in those cells with extreme velocities and negative water depth [7, 27]. However, this inevitably violates the mass and momentum conservation and locally destroys the solutions. Therefore, it is desirable to have a shallow flow model that automatically preserves non-negative water depth [1, 29]. As solute transport is considered in this work, the non-negativity should also apply to solute concentration.

Handling high roughness value is another challenging issue when solving the shallow water equations, especially when wet-dry interface is presented. Generally, implicit discretisation of the friction source terms may give better numerical stability. However, Burguete et al. [8] and Liang and Marche [29] found that implicit solution of the friction terms might not be adequate for maintaining non-negative water depth in applications involving wetting and drying over complex topography. Liang and Marche [29] proposed a splitting implicit scheme for evaluating the friction source terms. In their work, the magnitude of the friction force is also limited so that its maximum effect is to stop the fluid but not reverse it. The technique has been proved to be effective in providing stable and non-negative simulations.

In this work, the author aims to resolve the shallow flow driven solute transport problem by considering all the above challenging issues and present a model for dry-bed simulations over complex domain. The pre-balanced shallow water equations derived

by Liang and Borthwick [27] are extended to include the advection-diffusion equation and form a 4×4 hyperbolic system. The equations automatically provide well-balanced solutions to shallow flows occurring in a wet domain with complex topography and facilitate the applications to dry-bed cases. The pre-balanced governing equations are then solved by a second-order non-negative Godunov-type scheme. The paper is organised as follows. Following in Section 2, the governing equations are first introduced. Section 3 describes the numerical model. The numerical scheme is validated against several test cases in Section 4. At last, brief conclusions are drawn in Section 5.

2   Governing equations

In a matrix conservation form, the integrated shallow water and non-diffusive solute transport equations may be written as

$$\frac{\partial \mathbf{u}}{\partial t} + \frac{\partial \mathbf{f}}{\partial x} + \frac{\partial \mathbf{g}}{\partial y} = \mathbf{s}, \tag{2.1}$$

where t denotes time; x and y are the Cartesian coordinates; $\mathbf{u}$ is the flow variable vector; $\mathbf{f}$ and $\mathbf{g}$ are the flux vectors in the x and y-direction, respectively; $\mathbf{s}$ is the vector containing source terms. The vectors are defined as follows

$$\mathbf{u} = \begin{bmatrix} \eta \\ q_x \\ q_y \\ q_c \end{bmatrix}, \mathbf{f} = \begin{bmatrix} q_x \\ uq_x + \frac{g}{2}(\eta^2 - 2\eta z_b) \\ uq_y \\ uq_c \end{bmatrix}, \mathbf{g} = \begin{bmatrix} q_y \\ vq_x \\ vq_y + \frac{g}{2}(\eta^2 - 2\eta z_b) \\ vq_c \end{bmatrix}, \mathbf{s} = \begin{bmatrix} 0 \\ -\frac{\tau_{bx}}{\rho} - g\eta\frac{\partial z_b}{\partial x} \\ -\frac{\tau_{by}}{\rho} - g\eta\frac{\partial z_b}{\partial y} \\ s_c \end{bmatrix},$$

where η is the water surface elevation above the datum and z_b is the bottom elevation above the datum so that $h(=\eta - z_b)$ is the water depth; u and v are depth-averaged velocity components in the x and y-directions, respectively; g is the acceleration due to gravity; $q_x(=uh)$ and $q_y(=vh)$ are the uni-width discharges and $q_c(=ch)$ is the conservative solute concentration with c being the solute concentration; ρ is the water density; $-\partial z_b/\partial x$ and $-\partial z_b/\partial y$ represent the bed slopes in the two Cartesian directions; s_c is a source or sink term for the solute concentration; and τ_{bx} and τ_{by} are the bed friction stresses that may be estimated using the following empirical formulae

$$\tau_{bx} = \rho C_f u \sqrt{u^2 + v^2} \quad \text{and} \quad \tau_{by} = \rho C_f v \sqrt{u^2 + v^2}. \tag{2.2}$$

The bed roughness coefficient C_f is either prescribed or evaluated empirically from $C_f = gn^2/h^{1/3}$ with n being the Manning coefficient. The shallow water equations in (2.1) are derived to ensure well-balanced solutions for a wet-bed application [27,29].

The integrated shallow water and solute transport equations (2.1) form a 4×4 system of hyperbolic conservation laws and the flux Jacobian is given by

$$
\mathbf{A} = \frac{\partial \mathbf{F}}{\partial \mathbf{u}} =
\begin{bmatrix}
0 & n_x & n_y & 0 \\
(a^2 - u^2)n_x - uvn_y & 2un_x + vn_y & un_y & 0 \\
-uvn_x + (a^2 - v^2)n_y & vn_x & un_x + 2vn_y & 0 \\
-ucn_x - vcn_y & cn_x & cn_y & un_x + vn_y
\end{bmatrix},
\tag{2.3}
$$

where $\mathbf{F} = \mathbf{f}n_x + \mathbf{g}n_y$, n_x and n_y are the Cartesian components of the unit vector in the x and y-directions, respectively, and $a(= \sqrt{gh})$ is the wave celerity. The eigenvalues associated with the Jacobian $\mathbf{A}$ are

$$
\begin{aligned}
\lambda_1 &= un_x + vn_y - a, & \lambda_2 &= un_x + vn_y, \\
\lambda_3 &= un_x + vn_y, & \lambda_4 &= un_x + vn_y + a,
\end{aligned}
\tag{2.4}
$$

which are all real. This confirms the hyperbolicity of the foregoing 4×4 system of the shallow water and solute transport equations. The corresponding matrices for right and left eigenvectors are

$$
\mathbf{R} =
\begin{bmatrix}
1 & 0 & 0 & 1 \\
u - an_x & n_y & n_y & u + an_x \\
v - an_y & -n_x & -n_x & v + an_y \\
c & 1 & -1 & c
\end{bmatrix},
\tag{2.5}
$$

and

$$
\mathbf{L} = \frac{1}{2a}
\begin{bmatrix}
un_x + vn_y + a & -n_x & -n_y & 0 \\
van_x - uan_y - ca & an_y & -an_x & a \\
van_x - uan_y + ca & an_y & -an_x & -a \\
-un_x - vn_y + a & n_x & n_y & 0
\end{bmatrix}.
\tag{2.6}
$$

From the eigenstructure, it is evident that the behaviour of the species concentration is entirely analogous to the tangential velocity component (v for the x-split and u for the y-split shallow water equations), as suggested by Toro [39]. Therefore, the integrated equation set may be solved using a numerical scheme that is built for the shallow water equations.

3   Numerical model

The aforementioned integrated governing equations are solved herein by a finite volume Godunov-type scheme incorporated with the HLLC approximate Riemann solver. The numerical scheme is designed to ensure well-balanced and non-negative (in terms of both water depth and solute concentration) solutions for simulations involving wetting and drying over complex domain topography. Second-order accuracy is achieved by applying the MUSCL slope limited linear reconstruction [40] together with a Runge-Kutta time integration.

3.1 Godunov-type scheme

In a finite volume Godunov-type scheme, the following time-marching formula may be used to update the flow variables to a new time step:

$$\mathbf{u}_{i,j}^{n+1} = \mathbf{u}_{i,j}^{n} - \frac{\Delta t}{\Delta x}\left(\mathbf{f}_{i+1/2,j} - \mathbf{f}_{i-1/2,j}\right) - \frac{\Delta t}{\Delta y}\left(\mathbf{g}_{i,j+1/2} - \mathbf{g}_{i,j-1/2}\right) + \Delta t \mathbf{s}_{i,j}, \tag{3.1}$$

where the superscript n represents time level; subscripts i and j are the cell indexes; Δt is the time step; and Δx and Δy are the cell size in the x and y-direction, respectively. In order to update the flow variables, proper calculation of the interface fluxes ($\mathbf{f}_{i+1/2,j}$, $\mathbf{f}_{i-1/2,j}$, $\mathbf{g}_{i,j+1/2}$ and $\mathbf{g}_{i,j-1/2}$) and source terms ($\mathbf{s}_{i,j}$) is required in a well-balanced and non-negative Godunov-type framework. The numerical scheme has been presented elsewhere for solving the 1D shallow water equations [29]. In the following sub-sections, the numerical algorithm is reviewed and adapted for solving the aforementioned integrated shallow water and solute transport equations.

3.2 Flux calculation

A Godunov-type scheme solves local Riemann problems at each cell interface to evaluate interface fluxes. In this work, the HLLC approximate Riemann solver is chosen to solve these local Riemann problems due to its advantages in offering automatic entropy fix and easy treatment of wetting and drying. Compared with the original HLL approach, the HLLC approximate Riemann solver also presents major benefits in modelling two-dimensional flows, especially when the solute transport is included. Ignoring the middle wave, the two-wave assumption of the HLL Riemann solver is only correct for purely one-dimensional problems and may result in excessive smearing of contact discontinuities for multidimensional simulations [39]. In this work, the coupled two-dimensional shallow water and advection equations are considered and hence the HLLC solver should be used. Taking $\mathbf{f}_{i+1/2,j}$ as an example, the HLLC fluxes for the integrated governing equations may be defined as

$$\mathbf{f}_{i+1/2,j} = \begin{cases} \mathbf{f}_L & \text{if } 0 \leqslant S_L, \\ \mathbf{f}_{*L} & \text{if } S_L < 0 \leqslant S_M, \\ \mathbf{f}_{*R} & \text{if } S_M < 0 \leqslant S_R, \\ \mathbf{f}_R & \text{if } 0 > S_R, \end{cases} \tag{3.2}$$

where $\mathbf{f}_L = \mathbf{f}(\mathbf{q}_L)$ and $\mathbf{f}_R = \mathbf{f}(\mathbf{q}_R)$ are, respectively, the fluxes in the left and right regions of the Riemann solution structure, which are directly computed from the left and right Riemann states $\mathbf{q}_L$ and $\mathbf{q}_R$ defined at either side of the cell interface $i+1/2$; $\mathbf{f}_{*L}$ and $\mathbf{f}_{*R}$ are the fluxes in the middle region separated by the middle (contact) wave:

$$\mathbf{f}_{*L} = \begin{bmatrix} f_{*L1} \\ f_{*L2} \\ f_{*L3} \\ f_{*L4} \end{bmatrix} = \begin{bmatrix} f_{*1} \\ f_{*2} \\ v_L f_{*1} \\ c_L f_{*1} \end{bmatrix} \quad \text{and} \quad \mathbf{f}_{*R} = \begin{bmatrix} f_{*R1} \\ f_{*R2} \\ f_{*R3} \\ f_{*R4} \end{bmatrix} = \begin{bmatrix} f_{*1} \\ f_{*2} \\ v_R f_{*1} \\ c_R f_{*1} \end{bmatrix}, \tag{3.3}$$

where f denotes the individual entry of the flux vector $\mathbf{f}$, and f_{*1} and f_{*2} are calculated from the HLL formula [21]

$$\mathbf{f}_* = \frac{S_R \mathbf{f}_L - S_L \mathbf{f}_R + S_L S_R (\mathbf{q}_R - \mathbf{q}_L)}{S_R - S_L}, \tag{3.4}$$

where S_L, S_M and S_R are the left, middle and right wave speeds in the HLLC Riemann solution structure. Fraccarollo and Toro [16] and Toro [39] recommend the following formulae for estimating S_L and S_R to facilitate applications in wetting and drying:

$$S_L = \begin{cases} u_R - 2\sqrt{gh_R} & \text{if } h_L = 0, \\ \min\left(u_L - \sqrt{gh_L},\, u_* - \sqrt{gh_*}\right) & \text{if } h_L > 0, \end{cases} \tag{3.5}$$

and

$$S_R = \begin{cases} u_L + 2\sqrt{gh_L} & \text{if } h_R = 0, \\ \max\left(u_R + \sqrt{gh_R},\, u_* + \sqrt{gh_*}\right) & \text{if } h_R > 0, \end{cases} \tag{3.6}$$

where u_L, h_L, u_R and h_R are the velocity and depth components of the left and right Riemann states, u_* and h_* can be evaluated from [39]

$$u_* = \frac{1}{2}(u_L + u_R) + \sqrt{gh_L} - \sqrt{gh_R}, \tag{3.7}$$

and

$$h_* = \frac{1}{g} \left[\frac{1}{2} \left(\sqrt{gh_L} + \sqrt{gh_R} \right) + \frac{1}{4}(u_L - u_R) \right]^2. \tag{3.8}$$

For the middle wave speed S_M, Toro [39] suggests the following choice:

$$S_M = \frac{S_L h_R (u_R - S_R) - S_R h_L (u_L - S_L)}{h_R (u_R - S_R) - h_L (u_L - S_L)}. \tag{3.9}$$

3.3 Non-negative reconstruction of Riemann states

In the current finite volume scheme, flow variables are stored and updated at cell centres. This requires proper reconstruction of the Riemann states at either side of a cell interface in order to define the local Riemann problems and calculate the interface fluxes. Reconstructing the Riemann states in turn needs an appropriate approach to evaluate the face values of the flow variables at either side of the cell interface. In this work, the MUSCL slope limited linear reconstruction is used to estimate the face values, which is second-order accurate in space. At $i+1/2$, the left-hand-side face values are calculated by:

$$\overline{\mathbf{u}}^L_{i+1/2,j} = \mathbf{u}_{i,j} + \frac{\psi}{2}(\mathbf{u}_{i,j} - \mathbf{u}_{i-1,j}), \qquad \overline{h}^L_{i+1/2,j} = h_{i,j} + \frac{\psi_h}{2}(h_{i,j} - h_{i-1,j}),$$

$$\overline{z}^L_{bi+1/2,j} = \overline{\eta}^L_{i+1/2,j} - \overline{h}^L_{i+1/2,j}. \tag{3.10}$$

Herein ψ is the vector containing the slope limited functions for different flow variables [20], which is evaluated according to the flow data at cell (i,j) and its upwind and downwind neighbours $(i+1,j)$ and $(i-1,j)$. ψ_h is the slope limiter defined for water depth h. For better numerical stability, the minmod slope limiter is used in this work and it may be written for one of the flow variables as [22]:

$$\psi(r) = \max[0, \min(r, 1)], \tag{3.11}$$

where the ratio of successive gradient r is calculated against the flow variable under consideration. For example, r can be evaluated on a uniform grid for η from:

$$r = \frac{\eta_{i+1,j} - \eta_{i,j}}{\eta_{i,j} - \eta_{i-1,j}}. \tag{3.12}$$

r is defined in a similar way for h, q_x, q_y and q_c. The corresponding face values of velocity and solute concentration are then calculated accordingly by:

$$\overline{u}_{i+1/2,j}^L = \overline{q}_{x\,i+1/2,j}^L / \overline{h}_{i+1/2,j}^L, \quad \overline{v}_{i+1/2,j}^L = \overline{q}_{y\,i+1/2,j}^L / \overline{h}_{i+1/2,j}^L,$$
$$\overline{c}_{i+1/2,j}^L = \overline{q}_{c\,i+1/2,j}^L / \overline{h}_{i+1/2,j}^L. \tag{3.13}$$

The face values at the right hand side of $i+1/2$ can be defined similarly. The above slope limited linear reconstruction calculates face values for those wet cells away from the wet-dry front. In a dry cell or a wet cell directly adjacent to a dry cell, the face values are assumed to be the same as those at the cell centre. This essentially reduces the accuracy of the second-order scheme to first-order near the wet-dry interface but this is as expected after a slope limiting process.

Based on the above face values, the Riemann states of water depth are then defined as:

$$h_{i+1/2,j}^L = \max(0, \overline{\eta}_{i+1/2,j}^L - z_{bi+1/2,j}), \quad h_{i+1/2,j}^R = \max(0, \overline{\eta}_{i+1/2,j}^R - z_{bi+1/2,j}), \tag{3.14}$$

where $z_{bi+1/2,j}$ is single face value of bed elevation given by [1]:

$$z_{bi+1/2,j} = \max(\overline{z}_{bi+1/2,j}^L, \overline{z}_{bi+1/2,j}^R). \tag{3.15}$$

Obviously, (3.14) defines the effective water depth and ensures its non-negativity. The left Riemann states of other flow variables are then obtained accordingly:

$$\eta_{i+1/2,j}^L = h_{i+1/2,j}^L + z_{bi+1/2,j}, \qquad q_{xi+1/2,j}^L = \overline{u}_{i+1/2,j}^L h_{i+1/2,j}^L,$$
$$q_{yi+1/2,j}^L = \overline{v}_{i+1/2,j}^L h_{i+1/2,j}^L, \qquad q_{ci+1/2,j}^L = \overline{c}_{i+1/2,j}^L h_{i+1/2,j}^L, \tag{3.16}$$

and similarly for the right Riemann states. The above reconstruction of Riemann states does not affect the well-balancing property of the pre-balanced governing equations and well-balanced solutions can be directly obtained for wet-bed applications.

However, for a dry-bed application, a proper numerical technique must be designed to maintain the well-balancing property of the overall numerical scheme. After using the pre-balanced governing equations (2.1), the only situation that needs special consideration is the case generalized in Fig. 1, where a wet cell (i,j) shares a common interface $i+1/2$ with a dry cell $(i+1,j)$ at the discrete level and the bed elevation of the dry cell is higher than the water surface level at (i,j). At the common cell interface, the left and right face values of the flow variables and bed elevation are the same as those at the cell centres as the cell under consideration is either next to a dry cell or dry. The single face value of bed elevation is then given by

$$z_{bi+1/2,j} = \max(\overline{z}_{bi+1/2,j}^L, \overline{z}_{bi+1/2,j}^R) = \overline{z}_{bi+1/2,j}^R.$$

The aforementioned non-negative approach for constructing the Riemann states leads to $h_{i+1/2,j}^L = \max(0, \overline{\eta}_{i+1/2,j}^L - z_{bi+1/2,j}) = 0$ and, similarly, $h_{i+1/2,j}^R = 0$. Consequently the Riemann states of water level are reconstructed as

$$\eta_{i+1/2,j}^L = h_{i+1/2,j}^L + z_{bi+1/2,j} = z_{bi+1/2,j} \quad \text{and} \quad \eta_{i+1/2,j}^R = z_{bi+1/2,j}.$$

Therefore, the Riemann states of water level take the value of bed elevation $z_{bi+1/2,j}$, instead of the actual water surface elevation. Considering a steady state problem of lake at rest with $u = v \equiv 0$ but $h \neq 0$ in the wet areas, the still water surface should be exactly reproduced by a well-balanced numerical scheme. However, at the cell interface $i-1/2$, the Riemann states of water level is reconstructed as

$$\eta_{i-1/2,j}^L = \eta_{i-1/2,j}^R = \eta \equiv constant.$$

This essentially means that the fluxes through the cell interfaces $i-1/2$ and $i+1/2$ are computed based on η and $z_{bi+1/2,j}$, respectively. Therefore a net spurious momentum flux will be generated and the flux and source term balancing will be violated at cell (i,j). The still water is then driven into motion. In order to regain the well-balancing, Δz, the difference between the ground level (the numerical water level) and the actual water level at $i+1/2$, must be sought and subtracted from the corresponding face value of bed elevation and Riemann states of water surface:

$$z_{bi+1/2,j} \leftarrow z_{bi+1/2,j} - \Delta z, \quad \eta_{i+1/2,j}^L \leftarrow \eta_{i+1/2,j}^L - \Delta z, \quad \eta_{i+1/2,j}^R \leftarrow \eta_{i+1/2,j}^R - \Delta z, \tag{3.17}$$

and Δz is calculated by:

$$\Delta z = \max\left(0, z_{bi+1/2,j} - \overline{\eta}_{i+1/2,j}^L\right), \tag{3.18}$$

as illustrated in Fig. 1. After this local bed modification, $\eta_{i+1/2,j}^L = \eta_{i+1/2,j}^R = z_{bi+1/2,j} = \eta$, the well-balancing is regained. Equation (3.18) calculates a positive value only for a case similar to the one illustrated in Fig. 1; otherwise, it returns zero. Therefore, in implementing the numerical scheme, the local bed modification (3.17) and (3.18) applies to each cell interface in the domain and completes the non-negative reconstruction of Riemann states. They are then employed by the HLLC approximate Riemann solver to compute the interface fluxes $\mathbf{f}_{i+1/2,j}$. The Riemann states at the other cell interfaces and the corresponding fluxes $(\mathbf{f}_{i-1/2,j}, \mathbf{g}_{i,j+1/2}, \mathbf{g}_{i,j-1/2})$ are computed in an identical way.
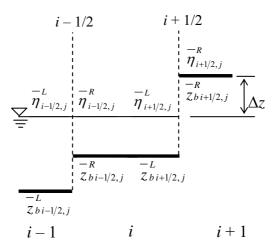
Figure 1: Constructing a well-balanced and non-negative scheme for dry-bed applications incorporating with local bed modification.

3.4 Discretization of source terms

In this work, the bed slope and friction source terms are treated separately. The bed slope source terms are approximated by a central difference approach compatible to the aforementioned flux calculation. In the x-direction,

$$-g\eta\frac{\partial z_b}{\partial x}=-g\bar{\eta}\left(\frac{z_{bi+1/2,j}-z_{bi-1/2,j}}{\Delta x}\right),\tag{3.19}$$

where $\bar{\eta}=(\eta^R_{i-1/2,j}+\eta^L_{i+1/2,j})/2$. Similar discretisation is applied to the y-direction. This simple discretisation of bed slope terms together with the above approach for flux calculation maintain the well-balancing of the numerical scheme, which can be easily proved by following the procedure detailed in Liang and Marche [29].

The friction source terms are evaluated using a splitting point-implicit scheme [9,15] for better stability. Detailed implementation of scheme in 1D, including the use of a limited friction force, is introduced in Liang and Marche [29] and extension to 2D is straightforward. Overall, in addition to preserving well-balanced solutions, the current Godunov-type numerical scheme maintains non-negativity of both water depth and solution concentration, as demonstrated later in the numerical experiments.

3.5 Second-order Runge-Kutta time integration

In order to obtain a second-order numerical scheme in time, a Runge-Kutta time integration method is employed and the time-marching formula (3.1) may be rewritten as

$$\mathbf{q}^{n+1}_{i,j}=\mathbf{q}^n_{i,j}+\frac{1}{2}\Delta t\left(\mathbf{K}_{i,j}(\mathbf{q}^n)+\mathbf{K}_{i,j}(\mathbf{q}^*)\right),\tag{3.20}$$

where $\mathbf{K}_{i,j}$ is the Runge-Kutta coefficient defined as

$$\mathbf{K}_{i,j} = -\frac{\mathbf{f}_{i+1/2,j} - \mathbf{f}_{i-1/2,j}}{\Delta x} - \frac{\mathbf{g}_{i,j+1/2} - \mathbf{g}_{i,j-1/2}}{\Delta y} + \mathbf{s}_{i,j}, \tag{3.21}$$

and $\mathbf{q}^*$ is the intermediate flow variables:

$$\mathbf{q}_{i,j}^* = \mathbf{q}_{i,j}^n + \Delta t \mathbf{K}_{i,j}(\mathbf{q}^n). \tag{3.22}$$

In order to update the flow variables to a new time step using (3.20), $\mathbf{K}_{i,j}(\mathbf{q}^n)$ and $\mathbf{K}_{i,j}(\mathbf{q}^*)$ must be computed separately in the two Runge-Kutta steps based on the aforementioned approaches for flux calculation and source term discretisation.

3.6 Stability criteria and boundary conditions

The current numerical scheme is overall explicit and a specific criterion must be in place to control the time step to ensure numerical stability. Because diffusion is excluded, a larger time step for solute transport based on the Courant-Friedrichs-Lewy (CFL) condition is allowed [2]. Therefore, in this work, the CFL criterion is used for predicting an appropriate time step Δt for a new iteration and the implementation is detailed in the author's previous work [27].

For all the test cases considered in this work, two types of boundary conditions, i.e. transmissive and solid, are used. For the transmissive boundary conditions, flow variables (η, q_x and q_y) at ghost points are provided so that zero gradients are calculated at the boundary. In the case of inlet or outlet boundary, the flow variables are directly prescribed according to the inflow and outflow requirements. In implementing the solid boundary conditions, the discharge (or velocity) and the gradient of water surface elevation (or water depth) must be zero at the boundary. The boundary condition for the solute concentration is imposed in the same way as water level (or depth), i.e. zero gradient must be enforced at the boundary point, no matter what type of boundary is being considered.

4 Results and discussion

The present numerical scheme for shallow flow driven solute transport is validated against several benchmark tests and results are compared with analytical solutions and alternative numerical predictions. $g = 9.81\text{m/s}^2$ and $\rho = 1000\text{kg/m}^3$ are used in all the tests and the Courant number for the CFL condition is set to 0.75.

4.1 Preservation of steady state related to a lake at rest

As discussed in the last section, the current numerical model is constructed to maintain well-balanced solutions even when wet-dry interface is present so that they can be applied in realistic simulations. Since diffusion is excluded, the preservation of steady state
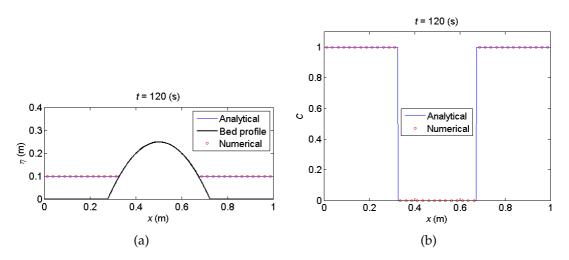
Figure 2: Still water test: comparison of numerical and analytical flow profiles along the domain central line at $t = 120$s (a) water surface elevation; (b) solute concentration.

equilibria related to a lake at rest should also include the solute concentration. Therefore the first test case is considered to demonstrate the new scheme's ability to preserve the still water level at a surface-piercing hump containing wet-dry interfaces. In a 1m × 1m closed domain, a hump is located at the centre with the bed topography defined by [6]:

$$z_b(x,y) = \max\lfloor 0, 0.25 - 5\left((x-0.5)^2 + (y-0.5)^2\right)\rfloor. \tag{4.1}$$
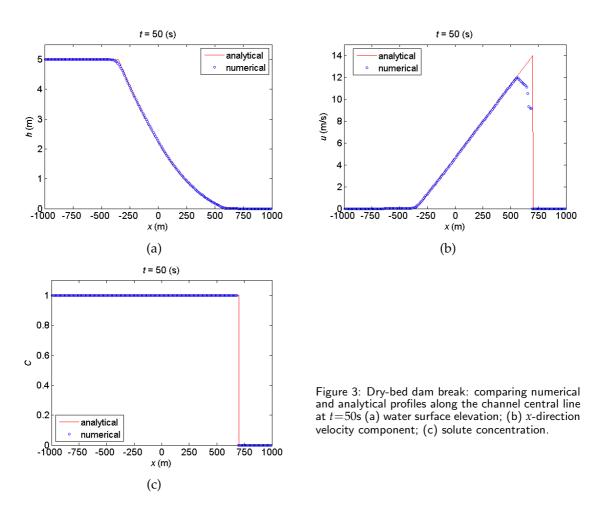
The still water level in the domain is 0.1m so that the island is partially submerged. The water is contaminated with the well-mixed solute concentration assumed to be 1. If the numerical scheme is well-balanced, these initial conditions should be exactly reproduced without numerical perturbation.

Simulations are run for 120s on several grids with different resolutions. In each case, the still water level as well as the solute concentration remains unchanged and the polluted water keeps perfectly tranquil. Fig. 2 presents the predicted profiles of water surface elevation and solute concentration along the central line of the domain for the simulation on a grid with 40 cells, where the initial conditions of the motionless flow are perfectly reproduced. Therefore, the well-balancing property of the current numerical scheme is confirmed.

4.2 Dam break on a frictionless dry bottom

The hydrodynamic problem of dam-break wave on a frictionless dry bottom was studied by Ritter [36] and analytical solutions were derived. This case was also recommended by the EU project of Concerted Action on Dam Break Modelling (CADAM) as one of the analytical tests for validating a shallow flow code.

The dam break takes place in a 2000m long channel. The channel is 200m wide but the channel width has no effect on the results as this is essentially a 1D test. A dam is located

(a)

(b)

(c)

Figure 3: Dry-bed dam break: comparing numerical and analytical profiles along the channel central line at t=50s (a) water surface elevation; (b) x-direction velocity component; (c) solute concentration.

1000m away from the upstream end and divides the channel into an upstream reservoir and a downstream dry valley. The 5m deep polluted water in the reservoir is originally motionless and the well-mixed solute has a concentration of 1. Because no diffusion is considered, the solute concentration is 1 wherever there is water and 0 over the dry bed and thus the analytical solution for q_c is the same as that of water depth in magnitude.

The simulation is carried out on a uniform grid with a resolution of 10m so that the grid contains 200 cells along the channel. Fig. 3(a) presents the numerical water depth plotting against the analytical solution at t=50s, where the rarefaction and wet-dry front are correctly reproduced. The predicted depth-averaged velocity is shown in Fig. 3(b) and agrees closely with the analytical solution in most of the domain but obvious discrepancy is found near to the front. This is due to the fact that the velocity is calculated as the ratio of the conserved flow variable q_x and water depth h. As the water depth vanishes near to the front, numerical errors may be exaggerated and cause the numerical velocity to deviate from the analytical solution. Fig. 3(c) demonstrates the solute concentration, which matches perfectly the analytical solution. No over or under-shoot is
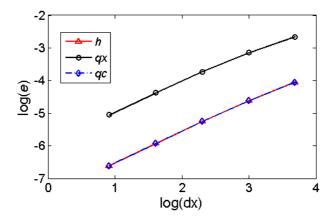
Figure 4: Dry-bed dam break: L1-error predicted for different flow variables on grids with different resolution.

predicted. In order to assess the convergence of the numerical scheme, simulations are also performed on another four uniform grids with different resolutions, i.e. $\Delta x = 2.5\text{m}$, 5m, 20m and 40m, respectively. The L1-error is calculated for h, q_x and q_c at $t = 50\text{s}$ and plotted against the cell size Δx in Fig. 4. The simulations are observed to converge at a rate of about 1. In this case, h and q_c have identical solutions and so the same L1-error. The results confirm the capability of the current numerical scheme on capturing wet-dry interface and predicting non-negative water depth and solution concentration.
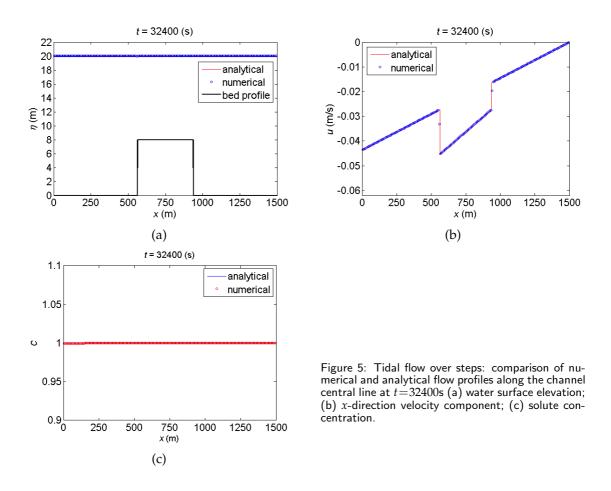
4.3 Tidal flow over steps

Also proposed by the EU CADAM project, the case of tidal flow over steps is a useful test for verifying the capability of a numerical scheme on dealing with discontinuous bed topography. The bed profile of the 1500m long frictionless channel where the tidal flow takes place is defined by

$$z_b(x) = \begin{cases} 8 & \text{if } |x-750| \leqslant 187.5, \\ 0 & \text{otherwise.} \end{cases} \tag{4.2}$$

This essentially provides two vertical steps at the middle of the domain. Asymptotic analytical solutions are available and given by [5]:

$$h(x,t) = 20 - z_b(x) - 4\sin\left[\pi\left(\frac{4t}{86400} + \frac{1}{2}\right)\right],$$
$$u(x,t) = \frac{(x-L)\pi}{5400h(x,t)}\cos\left[\pi\left(\frac{4t}{86400} + \frac{1}{2}\right)\right]. \tag{4.3}$$

In the current numerical scheme, the vertical steps are automatically approximated by very steep slopes that are equal to the ratio between the corresponding step height and grid size and no special treatment is implemented. During the simulation, the channel

(a)

(b)

(c)

Figure 5: Tidal flow over steps: comparison of numerical and analytical flow profiles along the channel central line at $t=32400$s (a) water surface elevation; (b) x-direction velocity component; (c) solute concentration.

is assumed to be 75m wide and discretised by a 200×10 uniform grid. The analytical solutions at $t=0$ are used to supply the initial conditions. The inflow driven by $h(0,t)$ is imposed at the western end while a solid wall is assumed at the eastern end of the channel.

Fig. 5 presents the numerical results at $t=32,400$s in terms of free-surface, velocity and concentration profiles along the central line of the channel. The numerical profiles are compared with the analytical solutions and excellent agreement is achieved. This proves that the current numerical scheme is able to provide accurate predictions for shallow flow applications involving complex and even discontinuous bed topography.

4.4 Long wave resonance in a parabolic basin

The analytical test of long wave resonance in a frictionless parabolic basin is considered herein to verify the current numerical model of solute transport in dealing with wetting and drying over a non-horizontal topography, which was also employed by Murillo et

al. [35] to validate their code. The bottom elevation of the parabolic basin is defined by

$$z_b(x,y) = h_{s0} \frac{r^2}{L^2}. \tag{4.4}$$

Herein r is the distance from the domain centre. h_{s0} is the still water depth at the domain centre and L represents the radius of the circular shoreline when the flow is in the motionless steady state. The analytical solution of the shallow water equations for this case was derived by Thacker [38] and the time varying water level is provided by:

$$\eta(r,t) = h_{s0} \left[\frac{(1-A^2)^{1/2}}{1-A\cos\omega t} - \frac{r^2}{L^2} \left(\frac{1-A^2}{(1-A\cos\omega t)^2} - 1 \right) \right], \tag{4.5}$$

where

$$A = \frac{L^4 - r_0^4}{L^4 + r_0^4} \quad \text{and} \quad \omega = \frac{1}{L}\sqrt{8gh_{s0}} \tag{4.6}$$

with r_0 being the distance from the domain centre to the point where the water depth is nil at $t=0$.

During the numerical simulation, the constants are chosen to be $h_{s0}=20$m, $r_0=1200$m and $L=1500$m in order to compare the results with those produced by Murillo et al. [35]. The computational domain is assumed to be 4000m × 4000m and discretised by a 100 × 100 uniform grid. At $t=0$, the water is still with the water surface distorted according to $\eta(r,0)$. Transmissive boundary conditions are imposed but the settings do not influence the results as the flow never reaches the domain boundary.

In order to validate the solute transport model, an initial solute concentration is assumed as:

$$c(r,0) = c_0 \exp\left(-\frac{r}{2r_0} \right), \tag{4.7}$$

where $c_0=1$ is used. As suggested by Murillo et al. [35], the distribution of solute concentration will return to its initial profile after integer number of oscillation period T because no diffusion is allowed, i.e.

$$c(r,t=KT) = c_0 \exp\left(-\frac{r}{2r_0} \right), \qquad K=1,\cdots,\infty. \tag{4.8}$$

Based on these settings, simulations are run for 4 periods and the results are presented in Fig. 6 to Fig. 9. Fig. 6 demonstrates the results in terms of water level profile at different output times. It is evident that the motion of the water surface is correctly simulated. The wet-dry interfaces are properly captured and no distortion is detected near the front which demonstrates the effectiveness of the current numerical technique in handling wetting and drying. It is also obvious from the results that the effect of numerical diffusion is negligible after 4 periods of simulation. Compared with those presented by
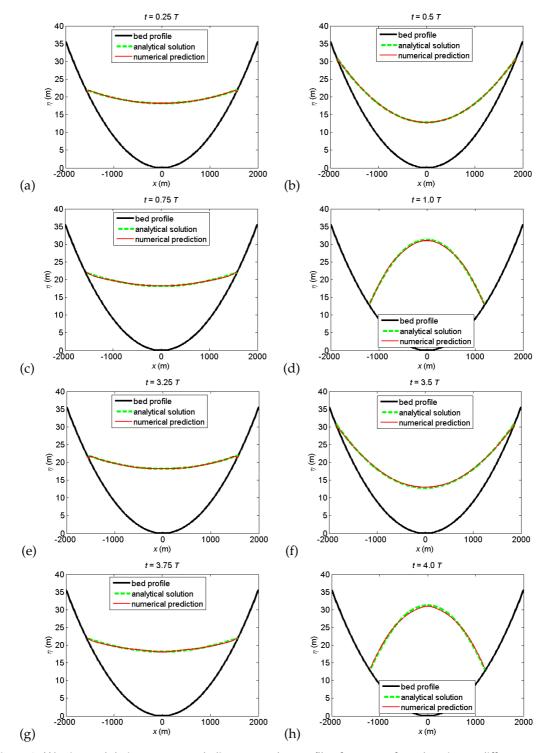
Figure 6: Wetting and drying over a parabolic topography: profile of water surface elevation at different output times (a) $t=0.25T$; (b) $t=0.5T$; (c) $t=0.75T$; (d) $t=1.0T$; (e) $t=3.25T$; (f) $t=3.5T$; (g) $t=3.75T$; (h) $t=4.0T$.
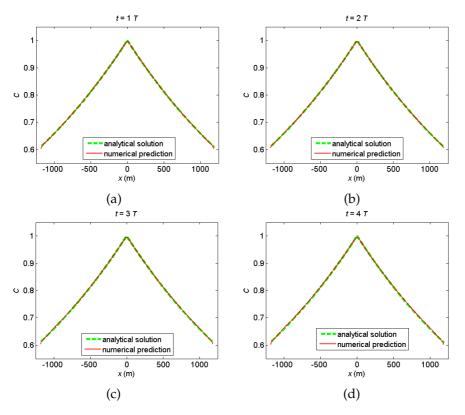
Figure 7: Wetting and drying over a parabolic topography: concentration profile at different output times (a) $t=1.0T$; (b) $t=2.0T$; (c) $t=3.0T$; (d) $t=4.0T$.

Murillo et al. [35], the current prediction provides a much better fit to the analytical solution throughout the simulation. Fig. 7 presents the profile of solute concentration along the x-direction central line of the domain at the end of each period. The numerical concentration profile matches nicely the analytical solution and again numerical diffusion does not have much influence on the results up to 4 periods. Fig. 9 presents the time histories of the oscillating water depth and the constant solute concentration at the domain centre, which confirms the above conclusions on the robustness and accuracy of the current model. The time history of the maximum and minimum solute concentration is illustrated in Fig. 9. Obviously the maximum solute concentration remains to be 1 while the minimum value is predicted to be 0 throughout the simulation. This means that the present numerical scheme predicts no over and under-shoot of the solute concentration and non-negativity and conservation of solute concentration is achieved.

In order to further demonstrate the accuracy of the current numerical model, simulations are run on three other uniform meshes with different resolution. The additional grids have resolution of $\Delta x = 10$m, 20m and 80m, respectively. The L1-error is calculated for η and q_c at the end of each simulation and plotted in Fig. 10 against the cell size Δx. The convergence rate for both η and q_c is about 1.4.

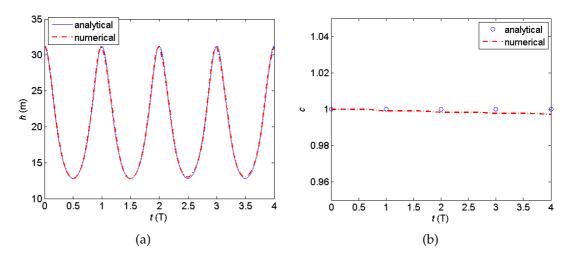(a)   (b)

Figure 8: Wetting and drying over a parabolic topography: time history of the key flow variables at the domain centre (a) water depth; (b) solute concentration.
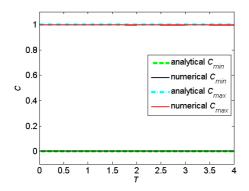

Figure 9: Wetting and drying over a parabolic topography: time history of the maximum and minimum values of concentration.

Figure 10: Wetting and drying over a parabolic topography: relative error calculated for different flow variables on grids with different resolution.

4.5 Dam break over three humps

Proposed by Kawahara and Umetsu [24], this case of dam break over three humps is a severe test for a shallow flow solver as it involves simultaneously discontinuous flow variables, repeating process of wetting and drying and relatively complex domain topography. Therefore it may be deemed as an idealised situation of a realistic dam-break problem. In a 75m × 30m rectangular domain, the bottom topography is provided by

$$
z_b(x,y) = \max\left(0, 1 - \frac{1}{8}\sqrt{(x-30)^2 + (y-6)^2},\right.
$$
$$
\left. 1 - \frac{1}{8}\sqrt{(x-30)^2 + (y-24)^2}, 3 - \frac{3}{10}\sqrt{(x-47.5)^2 + (y-15)^2}\right). \quad (4.9)
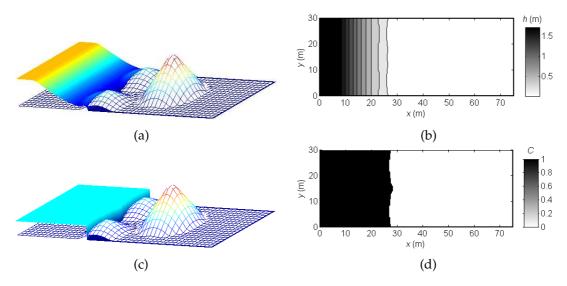$$

Figure 11: Dam break over three humps: numerical results at $t=2$s (a) 3D plot of water surface; (b) water depth contours; (c) 3D surface plot of solute concentration; (d) contours of solute concentration.

Initially, an infinitely thin dam is located at 16m away from the western end of the domain and the still water depth upstream the dam is 1.75m. The water is polluted with a well-mixed solute concentration of 1.

During the simulation, the domain is discretised by a 200×80 uniform grid and the Manning coefficient $n=0.018$ is used throughout the domain. Solid boundary conditions are imposed at the four lateral walls. The dam is removed immediately at $t=0$ and the simulation is run for 300s after the dam fails. Fig. 11 present the results at $t=2$s in terms of 3D surface plot and contours for both water depth and solute concentration. After the dam is removed, the polluted water rushes into the floodplain and at $t=2$s the front has reached and started to climb the two smaller humps at the front. Theoretically, the concentration of the solute is 1 wherever it is wet as diffusion is ignored. This is actually the case in the current simulation, as indicated in Figs. 11(c and d). Therefore, the sharp-fronted concentration is correctly simulated and no numerical diffusion is observed. Due to the huge momentum carried by the dam-break wave, the flow continues to travel rapidly downstream. After $t=6$s, as illustrated in Fig. 12, the dam-break flow has passed and submerged the two smaller humps. After hitting the big hump, the wave front has started to climb the big mound. Because of the blockage effect, only part of the flow is able to pass the big mound through the sides near the northern and southern boundary walls and continues to move downstream. The interaction among the violent dam-break wave, topography and boundary walls has caused a complex wave pattern. The sharp front of solute concentration coincides with the wet-dry interface and both are effectively modelled. At $t=12$s, as shown in Fig. 13, the dam-break wave makes its journey further downstream and those parts of front passing through the big mound are about to reach the downstream end of the domain. Due to the interaction between
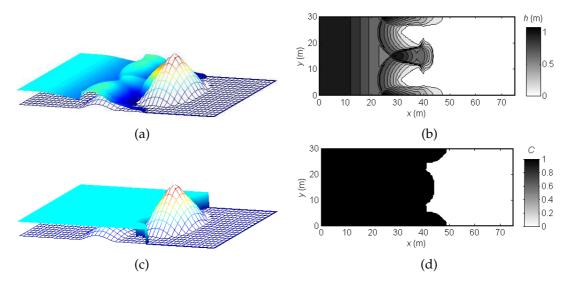
(a)   (b)

(c)   (d)

Figure 12: Dam break over three humps: numerical results at $t = 6$s (a) 3D plot of water surface; (b) water depth contours; (c) 3D surface plot of solute concentration; (d) contours of solute concentration.
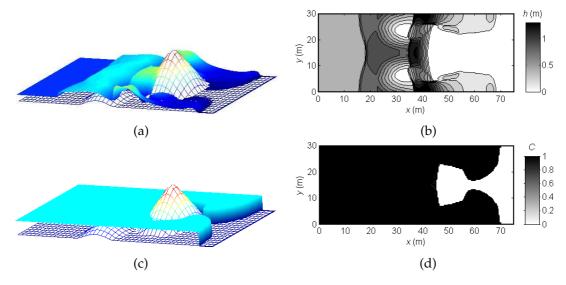

(a)   (b)

(c)   (d)

Figure 13: Dam break over three humps: numerical results at $t = 12$s (a) 3D plot of water surface; (b) water depth contours; (c) 3D surface plot of solute concentration; (d) contours of solute concentration.

the dam-break wave and the humps, a shock-wave has been generated and propagates backwards to the upstream boundary. Fig. 14 shows the results at $t = 30$s, in which the wet-dry front has reached the eastern boundary and another interacting shock has been created and moves upstream. This wave-topography-boundary interaction will continue until the momentum of the dam break is dissipated by the bed friction. Eventually the flow will settle down and become motionless again, as illustrated in Fig. 15 for $t = 300$s,
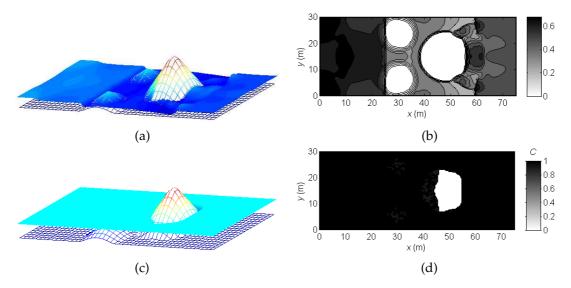
Figure 14: Dam break over three humps: numerical results at $t = 30$s (a) 3D plot of water surface; (b) water depth contours; (c) 3D surface plot of solute concentration; (d) contours of solute concentration.
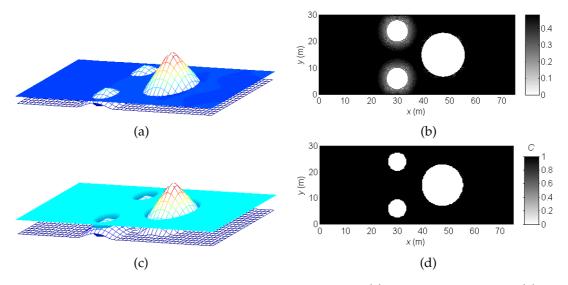

Figure 15: Dam break over three humps: numerical results at $t = 300$s (a) 3D plot of water surface; (b) water depth contours; (c) 3D surface plot of solute concentration; (d) contours of solute concentration.

where the top of the two smaller humps has become dry again. In all of the output times, the hydrodynamic behaviour of the dam-break wave and the complicated wetting and drying process are predicted to be similar to those obtained by Brufau et al. [6]. The solute concentration evolves according to the development of the flow and the discontinuous front is always properly captured. Fig. 16 presents the time history of the maximum and minimum solute concentration. Again, the two extreme values remain to be 1 and
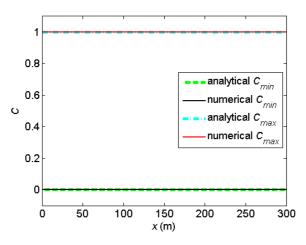
Figure 16: Dam break over three humps: time history of the maximum and minimum values of concentration.

0 throughout the simulations in this severe test. Including most of the features for a realistic dam-break problem, successfully handling of this case essentially indicates the potential of the current model in real-world applications.

5 Conclusions

Solute transport is an important topic in shallow flow modelling. This paper presents a robust model for simulating shallow flow induced solute transport process. The model is based on the finite volume Godunov-type solution to the integrated 4×4 hyperbolic conservation laws consisting of the shallow water and solute transport equations. The second-order accurate Godunov-type model is constructed using a well-balanced and non-negative scheme. Well-balanced solution to the problem of lake at rest is automatically achieved for wet-bed simulations after employing a set of pre-balanced governing equations. For applications involving wetting and drying over complex topography, the numerical scheme is carefully designed to ensure non-negativity in terms of both water depth and solute concentration. A local bed modification method is implemented together with the non-negative reconstruction to maintain well-balancing for dry-bed applications. Compatible to the non-negative reconstruction, a central difference scheme is directly used for discretising the bed-slope source terms. The friction source terms are solved by a splitting limited implicit scheme to ensure numerical stability near the wet-dry interface. As a whole, the current numerical scheme is effective in providing well-balanced and non-negative solutions to complex shallow flow driven solute transport problems involving wetting and drying over irregular domain topography. Meanwhile, it is straightforward to understand and easy to implement. There is no need of any clipping treatment to amend the flow variables in order to maintain positivity of water depth and solute concentration. So the numerical scheme provides better conservative property

than most of the alternative approaches reported in literature [35]. It should be noted that the diffusion term in the solution transport equation is ignored in the current numerical scheme. In lots of applications involving wetting and drying, the flow evolves rapidly and the diffusion effect is relatively small compared to advection. However, if it is necessary, the diffusion terms can be easily included in the governing equations and solved by central differences [28] or an implicit scheme for better numerical stability as suggested by Murillo et al. [34]. For applications involving irregular domain boundaries, the current model can be directly combined with the Cartesian cut-cell technique [11, 30] or the simple boundary treatment method proposed by Liang and Borthwick [26] to provide curved boundary treatment.

The present solute transport model is validated against four analytical benchmarks and then applied to simulate a more realistic test of dam break over three humps. In all of the cases being investigated, the numerical predictions compare well with the analytical solutions or alternative numerical results reported in literature. Evolution of mass for both water and solute concentration is monitored throughout the simulations and absolute conservation is observed for all the tests, which is as expected for the current numerical scheme. Furthermore, non-negative and maximum concentration principles are guaranteed for pollutant transport, i.e. no under or over-shoot is predicted throughout all the simulations. The last case of dam break over three humps is a severe test involving flow discontinuity, wetting and drying and complex domain topography, which are the most important elements in a realistic shallow flow problem. Successful handling of this case indicates that the current model is directly applicable to real-world applications of solute transport driven by shallow flows, e.g. the propagation of sewage waste during a flood event.

Acknowledgments

References

[1] E. Audusse, F. Bouchut, M.-O. Bristeau, R. Klein, and B. Perthame. A fast and stable well-balanced scheme with hydrostatic reconstruction for shallow water flows. SIAM Journal on Scientific Computing, 25(6):2050-2065, 2004.
[2] E. Audusse, and M.-O. Bristeau. Transport of pollutant in shallow water - a two time steps kinetic method. M2AN Mathematical Modelling and Numerical Analysis, 37(2):389-416, 2003.
[3] L. Begnudelli, and B.F. Sanders. Unstructured grid finite-volume algorithm for shallow-water flow and scalar transport with wetting and drying. ASCE Journal of Hydraulic Engineering, 132(4):371-384, 2006.
[4] F. Benkhaldoun, I. Elmahi, and M. Seaïd. Well-balanced finite volume schemes for pollutant transport by shallow water equations on unstructured meshes. Journal of Computational Physics, 226(1):180-203, 2007.

[5] A. Bermúdez, and M.E. Vázquez. Upwind methods for hyperbolic conservation laws with source terms. Computers & Fluids, 8:1049-1071, 1994.

[6] P. Brufau, P. García-Navarro, and M.E. Vázquez-Cendón. A numerical model for the flooding and drying of irregular domains. International Journal for Numerical Methods in Fluids, 39:247-275, 2002.

[7] P. Brufau, P. García-Navarro, and M.E. Vázquez-Cendón. Zero mass error using unsteady wetting-drying conditions in shallow flows over dry irregular topography. International Journal for Numerical Methods in Fluids, 45:1047-1082, 2004.

[8] J. Burguete, P. García-Navarro, and J. Murillo. Friction term discretization and limitation to preserve stability and conservation in the 1D shallow-water model: application to unsteady irrigation and river flow. International Journal for Numerical Methods in Fluids, 58:403-425, 2008.

[9] T.R.A. Bussing, and E.M. Murman. Finite volume method for the calculation of compressible chemically reacting flows. AIAA Journal, 26(9):1070-1078, 1988.

[10] D. Calhoun, R.J. LeVeque. A Cartesian grid finite-volume method for the advection-diffusion equation in irregular geometries. Journal of Computational Physics, 157(1):143 - 180, 1999.

[11] D.M. Causon, D.M. Ingram, C.G. Mingham, G. Yang, and R.V. Pearson. Calculation of shallow water flows using a Cartesian cut cell approach. Advances in Water Resources, 23(5):545-562, 2000.

[12] A. Chertock, A. Kurganov, and G. Petrova. Finite-volume-particle methods for models of transport of pollutant in shallow water. Journal of Scientific Computing, 27(1-3):189-199, 2006.

[13] N. Dodd. A numerical model of wave run-up, overtopping and regeneration. ASCE Journal of Waterway, Port, Coastal and Ocean Engineering, 124(2):73-81, 1998.

[14] R.A. Falconer. Flow and water quality modelling in coastal and inland waters. Journal of Hydraulic Research, 30:437-452, 1992.

[15] F.R. Fiedler, and J.A. Ramirez. A numerical method for simulating discontinuous shallow flow over an infiltrating surface. International Journal for Numerical Methods in Fluids, 32(2):219-239, 2000.

[16] L. Fraccarollo, and E.F. Toro. Experimental and numerical assessment of the shallow water model for two-dimension dam-break type problems. Journal of Hydraulic Research, 33(6):843-863, 1995.

[17] P. García-Navarro, E. Playán, and N. Zapata. Solute transport modelling in overland flow applied to fertigation. ASCE Journal of Irrigation and Drainage Engineering, 126(1):33-40, 2000.

[18] P. García-Navarro, and M.E. Vázquez-Cendón. On numerical treatment of the source terms in the shallow water equations. Computers & Fluids, 29:951-979, 2000.

[19] J.M. Greenberg, and A.-Y. LeRoux. A well-balanced scheme for the numerical processing of source terms in hyperbolic equations. SIAM Journal on Numerical Analysis, 33:1-16, 1996.

[20] A. Harten, B. Engquist, S. Osher, and S.R. Chakravarthy. Uniformly high order accurate essentially non-oscillatory schemes. Journal of Computational Physics, 71: 231-303, 1987.

[21] A. Harten, P.D. Lax, and B. van Leer. On upstream differencing and Godunov-type schemes for hyperbolic conservation-laws. SIAM Review, 25(1):35-61, 1983.

[22] C. Hirsch. Numerical Computation of Internal and External Flows. Vol. 2: Computational Methods for Inviscid and Viscous Flows. New York: Wiley, 1990.

[23] M.E. Hubbard, and P. García-Navarro. Flux difference splitting and the balancing of source

terms and flux gradients. Journal of Computational Physics, 165(1):89-125, 2000.

[24] M. Kawahara, and T. Umetsu. Finite element method for moving boundary problems in river flow. International Journal for Numerical Methods in Fluids, 6:365-86, 1986.

[25] R.J. LeVeque. Balancing source terms and flux gradients in high-resolution Godunov methods: the quasi-steady wave-propagation algorithm. Journal of Computational Physics, 146(1):346-365, 1998.

[26] Q. Liang, and A.G.L. Borthwick. Simple treatment of non-aligned boundaries in a Cartesian grid shallow flow model. International Journal for Numerical Methods in Fluids, 56(11):2091-2110, 2000.

[27] Q. Liang, and A.G.L. Borthwick. Adaptive quadtree simulation of shallow flows with wet-dry fronts over complex topography. Computers & Fluids, 38(2):221-234, 2009.

[28] Q. Liang, A.G.L. Borthwick, P.H. Taylor, and J. Huang. Godunov-type quadtree model of species dispersion in shallow flows. Proceedings of the International Symposium on Shallow Flows. 16-18 June 2003, Delft University of Technology, The Netherlands, 2003.

[29] Q. Liang, and F. Marche. Numerical resolution of well-balanced shallow water equations with complex source terms. Advances in Water Resources, 32(6):873-84, 2009.

[30] Q. Liang, J. Zang, A.G.L. Borthwick, and P.H. Taylor. Shallow flow simulation on dynamically adaptive cut-cell quadtree grids. International Journal for Numerical Methods in Fluids, 53(12):1777-1799, 2007.

[31] C. Man, and C.W. Tsai. A higher-order predictor-corrector scheme for two-dimensional advection-diffusion equation. International Journal for Numerical Methods in Fluids, 56:401-418, 2008.

[32] C.G. Mingham, and D.M. Causon. Calculation of unsteady bore diffraction using a high resolution finite volume scheme. Journal of Hydraulic Research, 38(1):49-56, 2000.

[33] C.G. Mingham, and D.M. Causon. A simple high-resolution advection scheme. International Journal for Numerical Methods in Fluids. 56:469-484, 2008.

[34] J. Murillo, J. Burguete, P. Brufau, and P. Carcía-Navarro. Coupling between shallow water and solute flow equations: analysis and management of source terms in 2D. International Journal for Numerical Methods in Fluids, 49:267-299, 2005.

[35] J. Murillo, P. Carcía-Navarro, J. Burguete, and P. Brufau. A conservative 2D model of inundation flow with solute transport over dry bed. International Journal for Numerical Methods in Fluids, 52:1059-1092, 2006.

[36] A. Ritter. Die Fortpflanzung der Wasserwellen: Zeitschrift des Vereines Deutscher Ingenieure, 36(33):947-954, 1892.

[37] B.D. Rogers, A.G.L. Borthwick, and P.H. Taylor. Mathematical balancing of flux gradient and source terms prior to using Roe's approximate Riemann solver. Journal of Computational Physics, 192(2):422-451, 2003.

[38] W.C. Thacker. Some exact solutions to the nonlinear shallow water equations. Journal of Fluid Mechanics, 107:499-508, 1981.

[39] E.F. Toro. Shock-capturing methods for free-surface shallow flows. Chichester: John Wiley & Sons, 2001.

[40] B. van Leer. Towards the ultimate conservative difference scheme. V - A second-order sequel to Godunov's method. Journal of Computational Physics, 32:101-136, 1979.

[41] M.E. Vázquez-Cendón. Improved treatment of source terms in upwind schemes for the shallow water equations in channels with irregular geometry. Journal of Computational Physics, 148(2):497-526, 1999.

[42] D.H. Zhao, H.W. Shen, G.Q. Tabious III, S.J. Lai, and W.Y. Tan. Finite-volume two-

dimensional unsteady-flow model for river basins. ASCE Journal of Hydraulic Engineering, 120(7):864-883, 1994.

[43] J.G. Zhou, D.M. Causon, C.G. Mingham, and D.M. Ingram. The surface gradient method for the treatment of source terms in the shallow-water equations. Journal of Computational Physics, 168(1):1-25, 2001.

[44] J.G. Zhou, D.M. Causon, C.G. Mingham, and D.M. Ingram. Numerical prediction of dam-break flows in general geometries with complex bed topography. ASCE Journal of Hydraulic Engineering, 130(4):332-340, 2004.